

Supporting Information

Synthesis of Nickel and Palladium Complexes with Diarylamido-based Unsymmetrical Pincer Ligands and Application for Norbornene Polymerization

Hui Liu, Haibin Yuan, and Xiaochao Shi*

*Department of Polymer Materials, Collede of Materials Science and Engineering,
Shanghai University, Materials Building, Nanchen Street 333, Shanghai 200444,
China. E-mail: xcshi@shu.edu.cn*

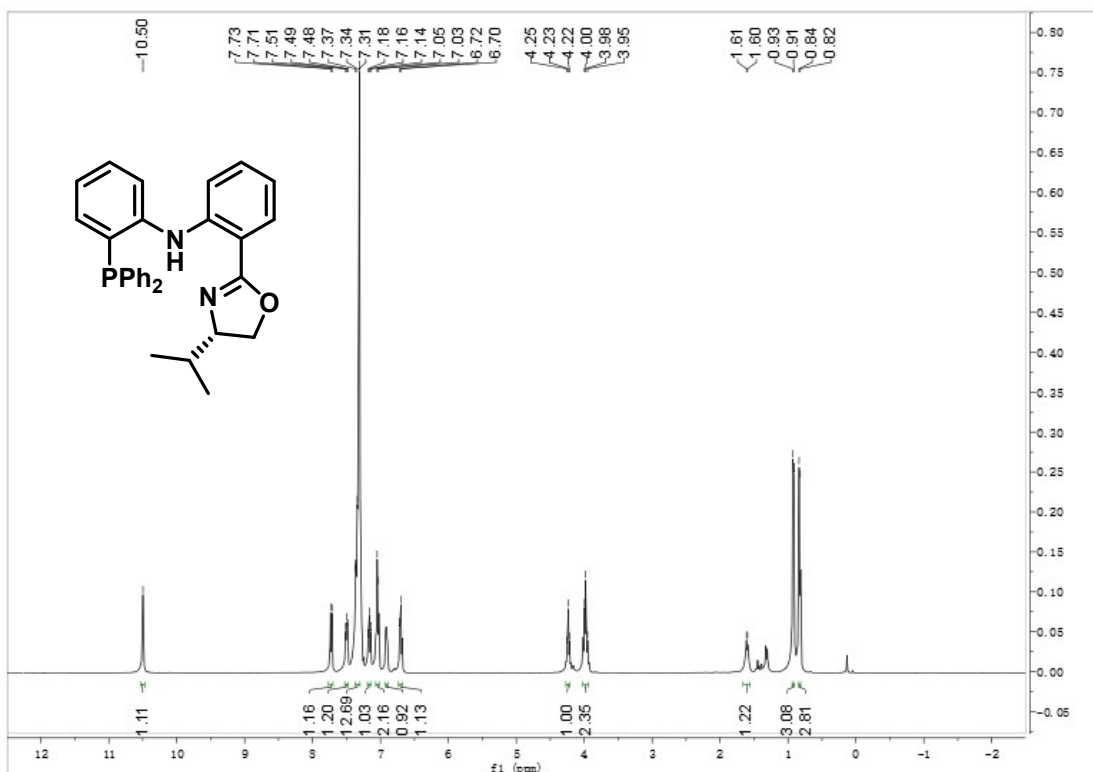


Figure S1 ¹H NMR spectrum of L1 (400 MHz, CDCl₃, 25 °C)

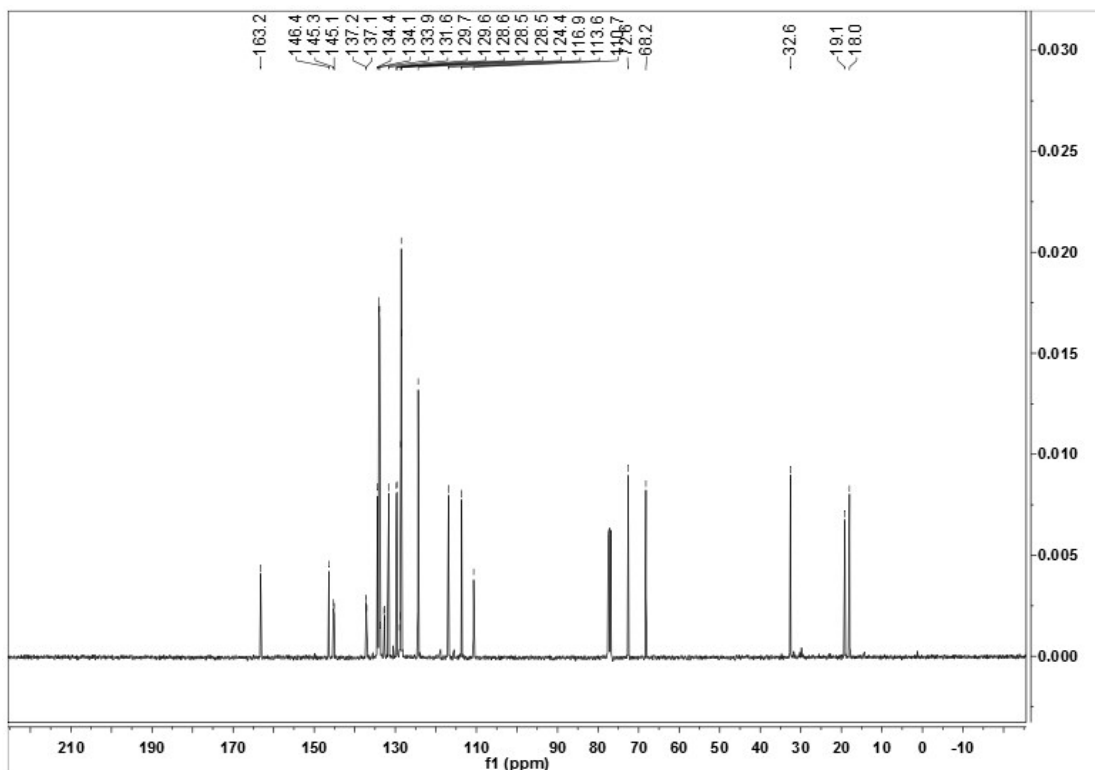


Figure S2 ¹³C NMR spectrum of L1 (101 MHz, CDCl₃, 25 °C)

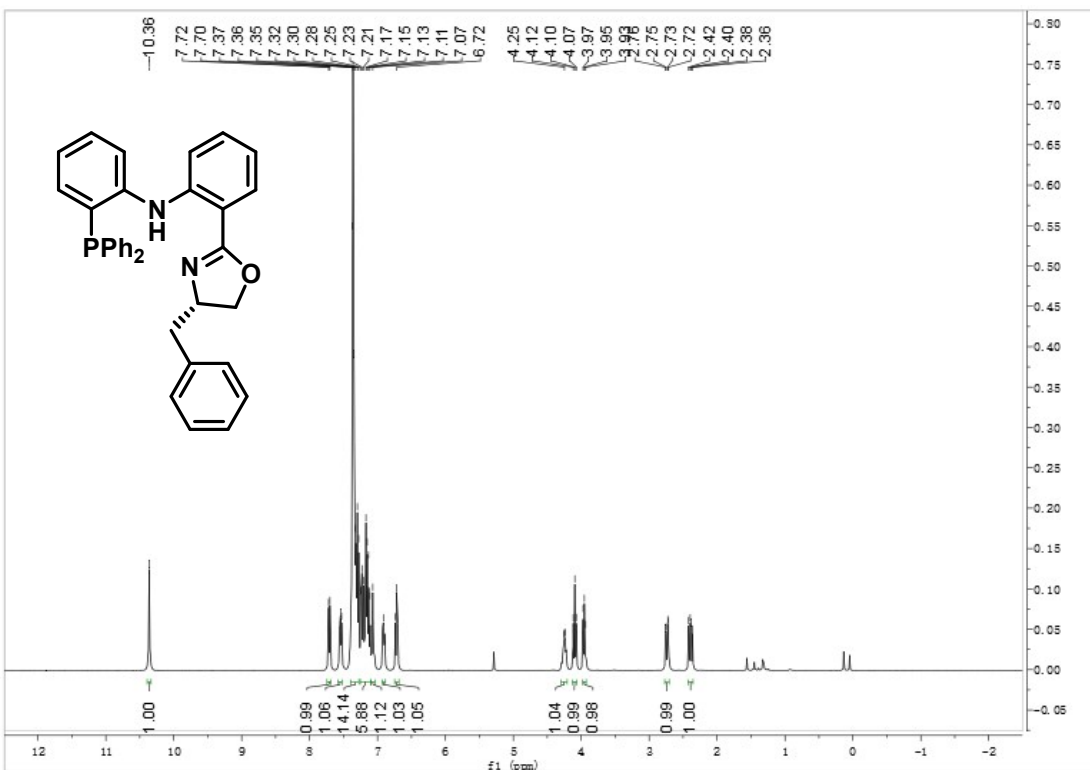


Figure S3 ¹H NMR spectrum of L2 (400 MHz, CDCl₃, 25 °C)

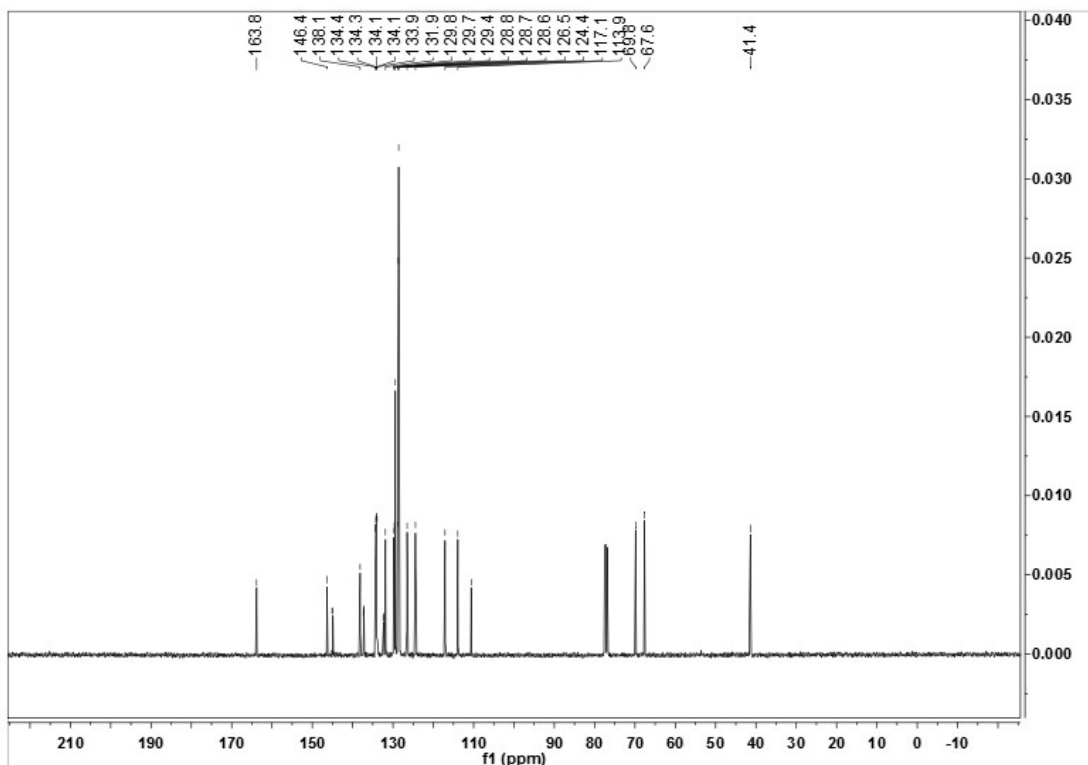


Figure S4 ¹³C NMR spectrum of L2 (101 MHz, CDCl₃, 25 °C)

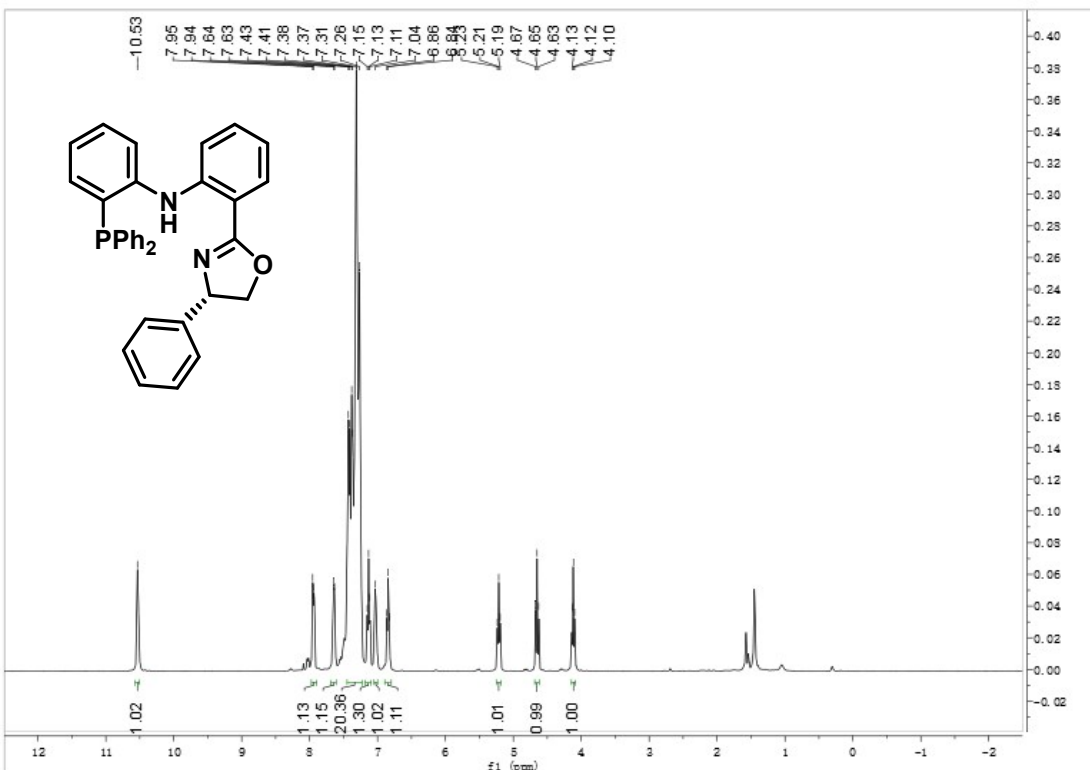


Figure S5 ¹H NMR spectrum of L3 (400 MHz, CDCl₃, 25 °C)

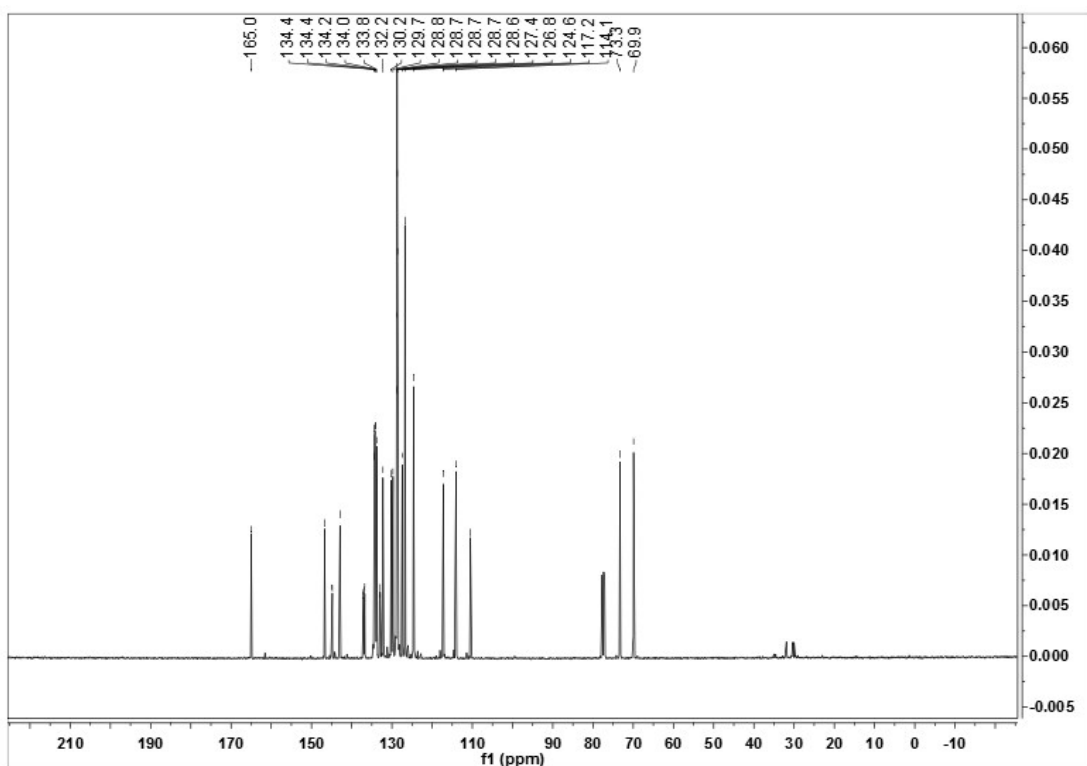


Figure S6 ¹³C NMR spectrum of L3 (101 MHz, CDCl₃, 25 °C)

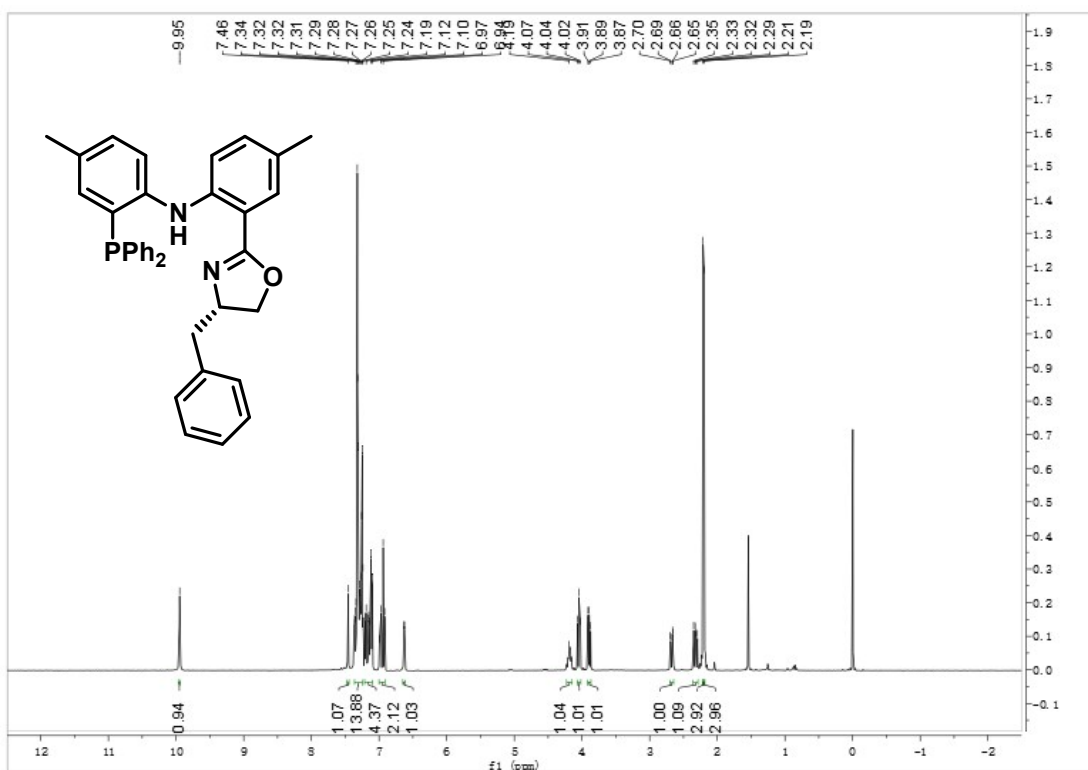


Figure S7 ^1H NMR spectrum of **L4** (400 MHz, CDCl_3 , 25 °C)

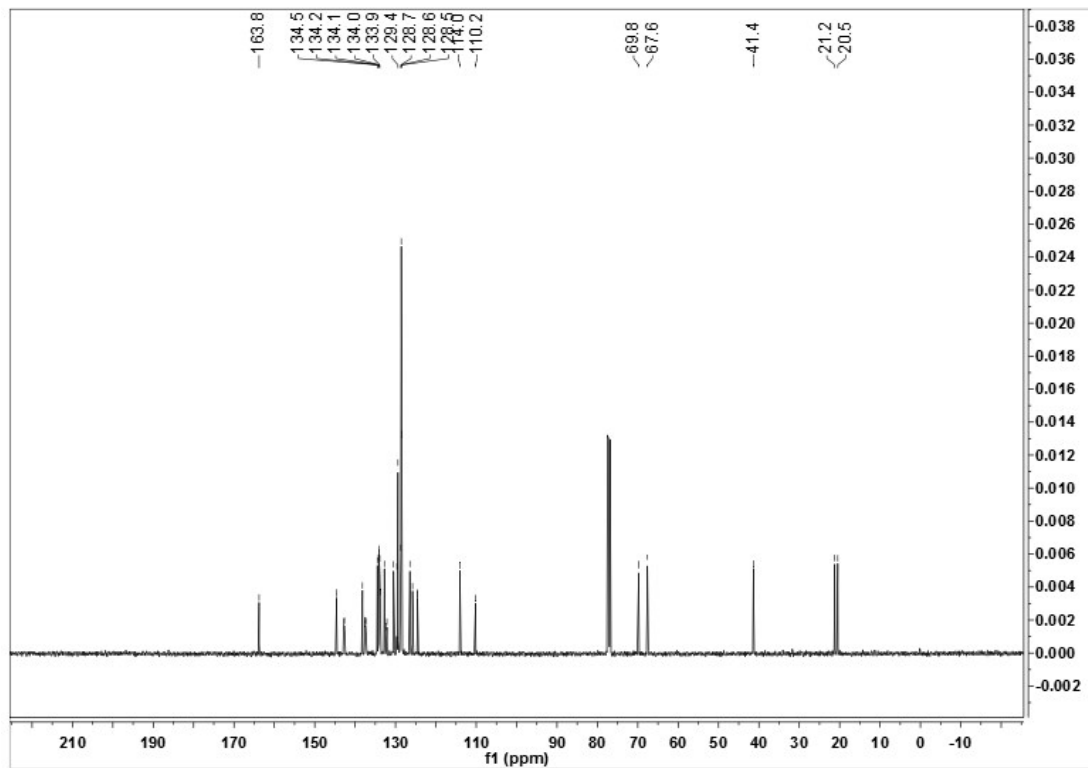


Figure S8 ^{13}C NMR spectrum of L4 (101 MHz, CDCl_3 , 25 °C)

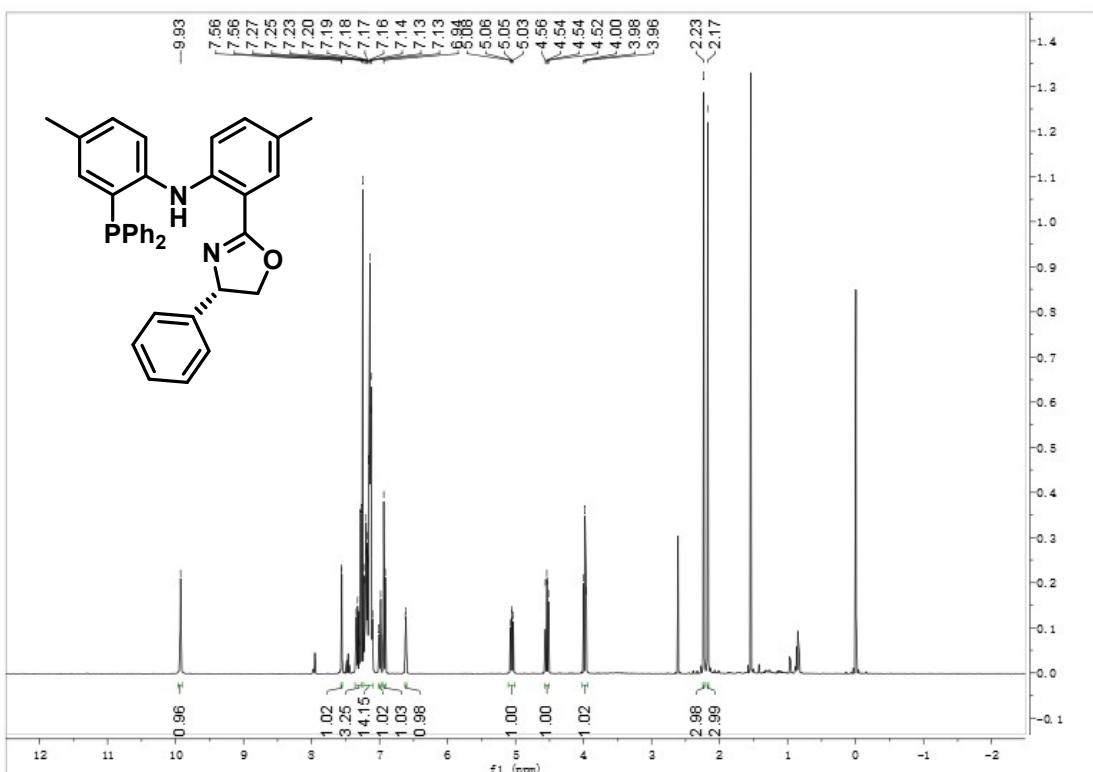


Figure S9 ¹H NMR spectrum of L5 (400 MHz, CDCl₃, 25 °C)

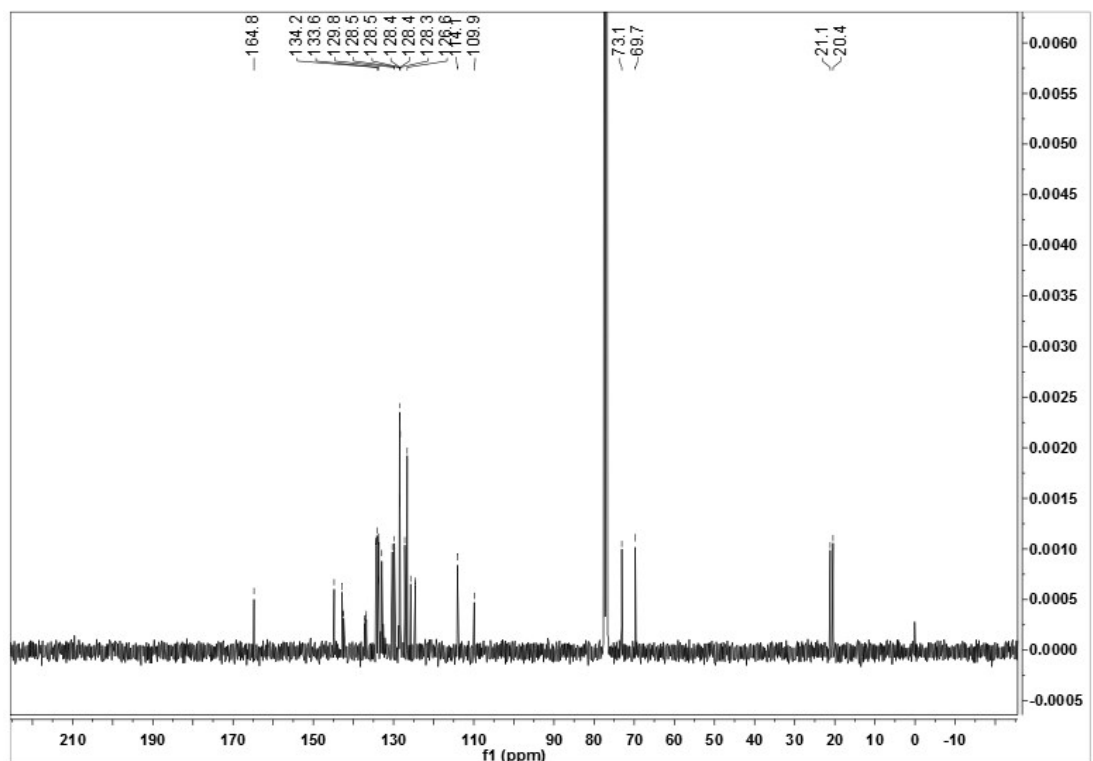


Figure S10 ¹³C NMR spectrum of L5 (101 MHz, CDCl₃, 25 °C)

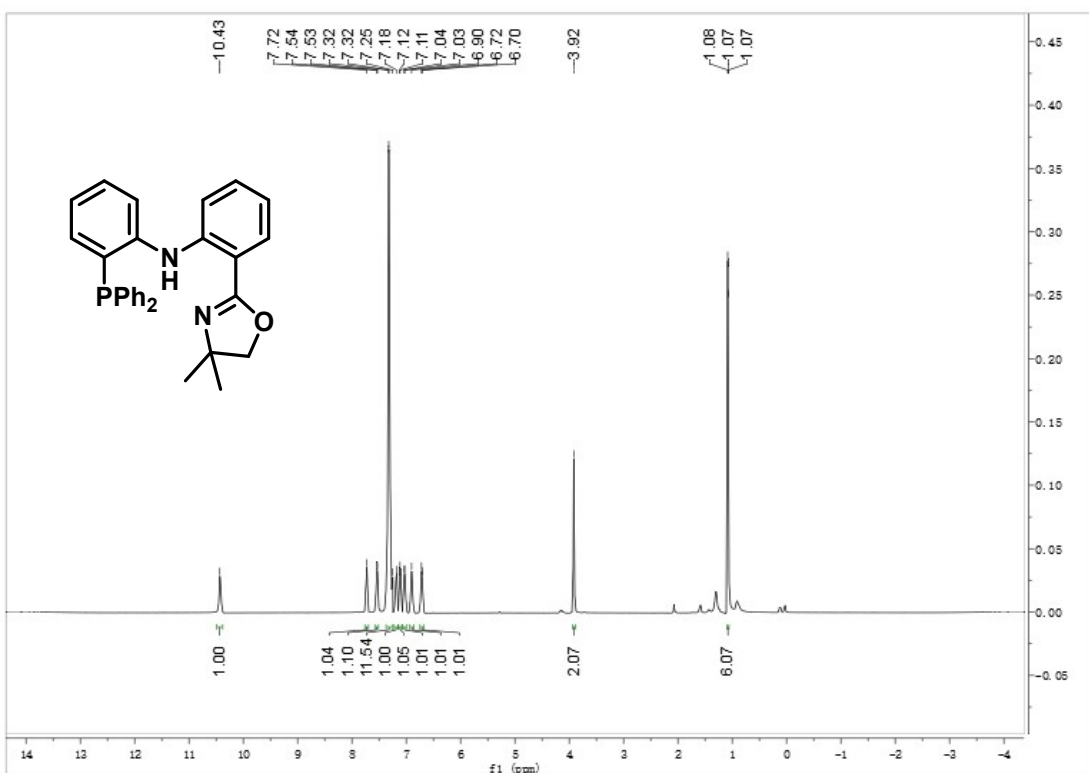


Figure S11 ^1H NMR spectrum of L6 (400 MHz, CDCl_3 , 25 °C)

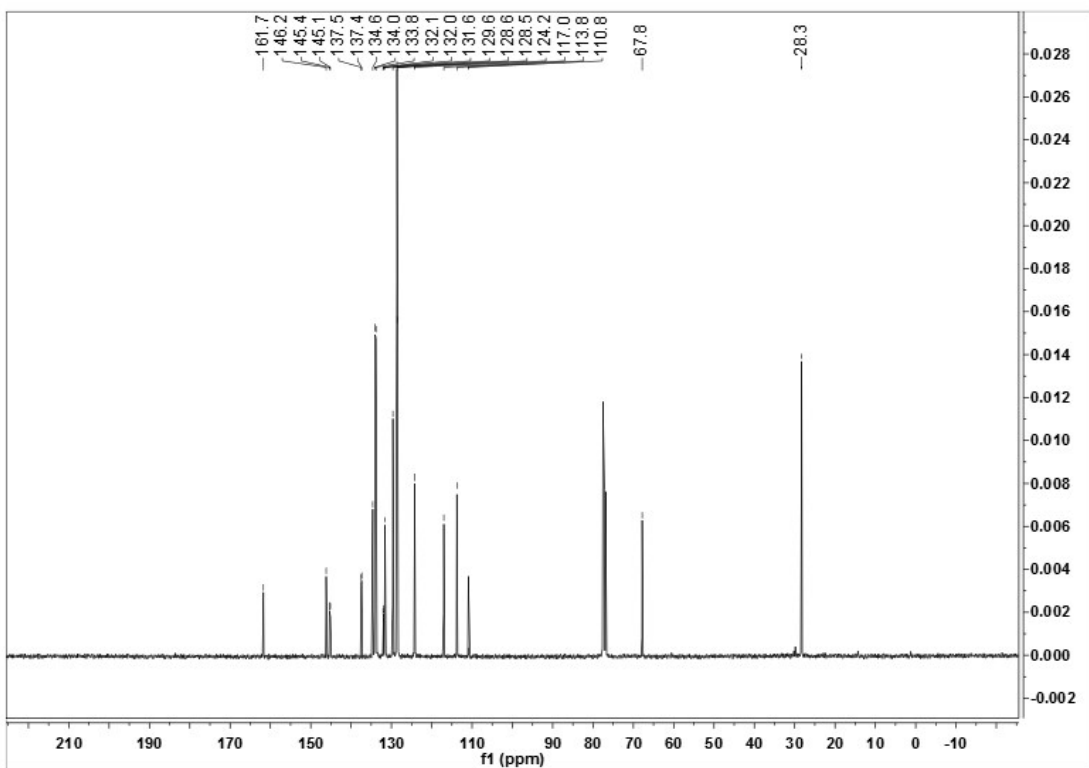


Figure S12 ^{13}C NMR spectrum of L6 (101 MHz, CDCl_3 , 25 °C)

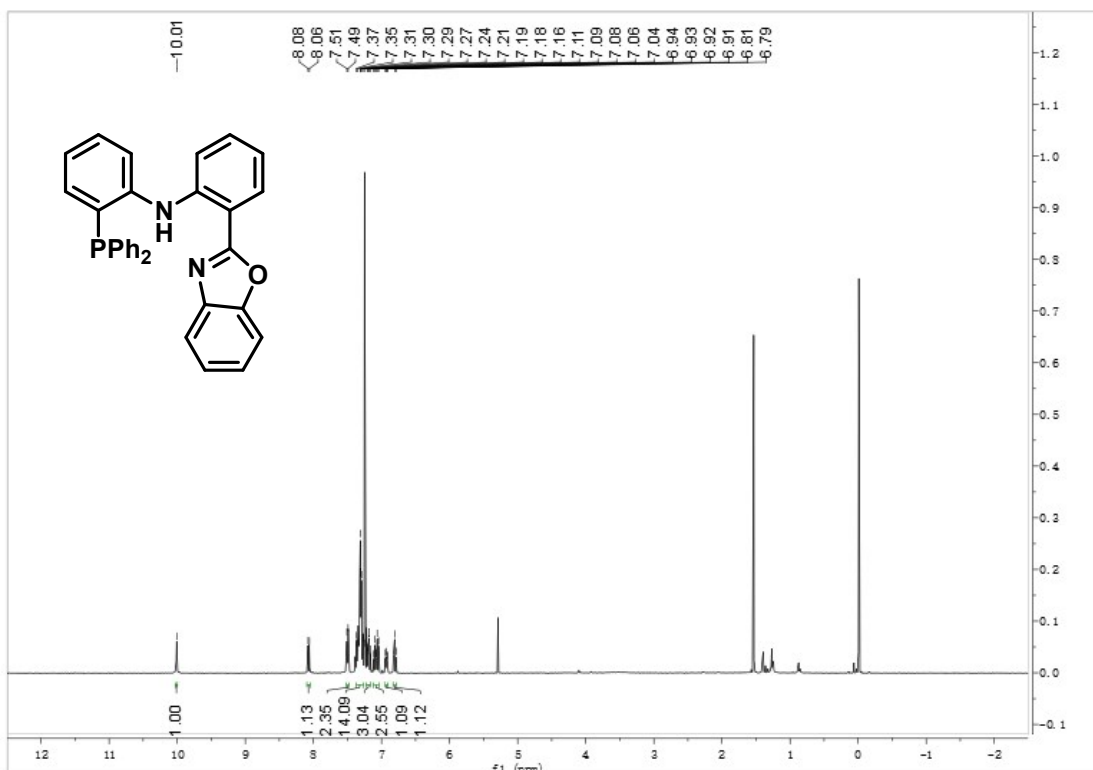


Figure S13. ^1H NMR spectrum of **L7** (400 MHz, CDCl_3 , 25°C)

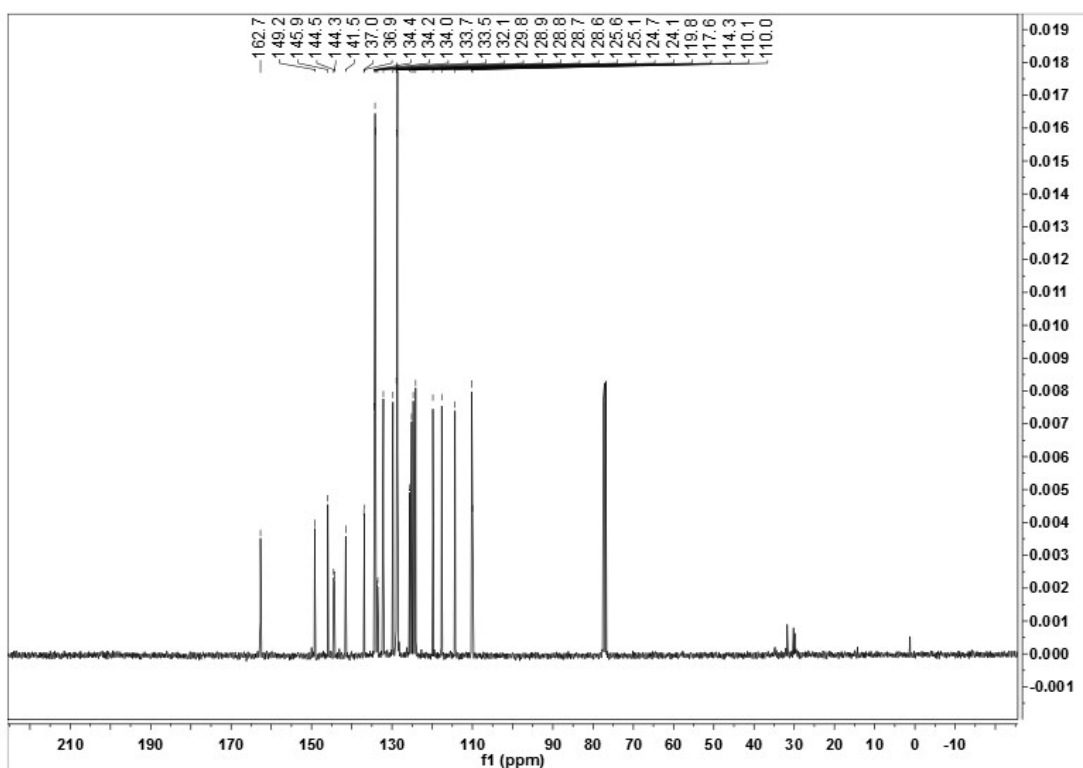


Figure S14 ^{13}C NMR spectrum of **L7** (101 MHz, CDCl_3 , 25 °C)

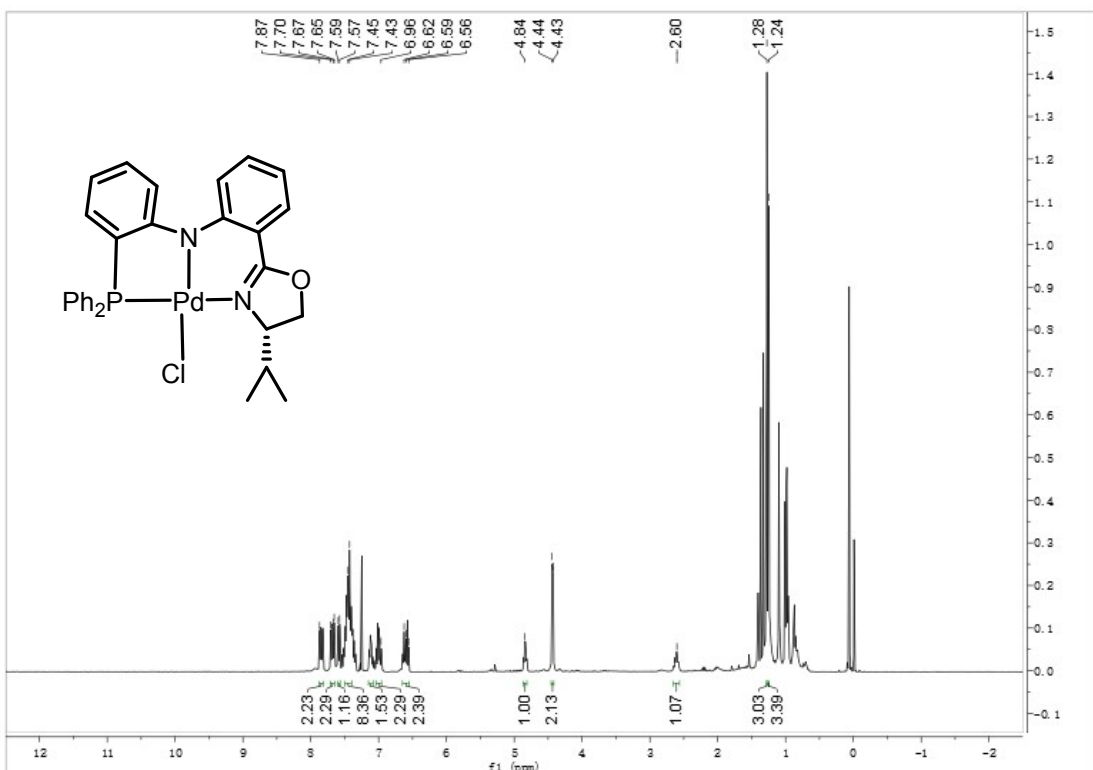


Figure S15 ^1H NMR spectrum of **Pd1** (400 MHz, CDCl_3 , 25 °C)

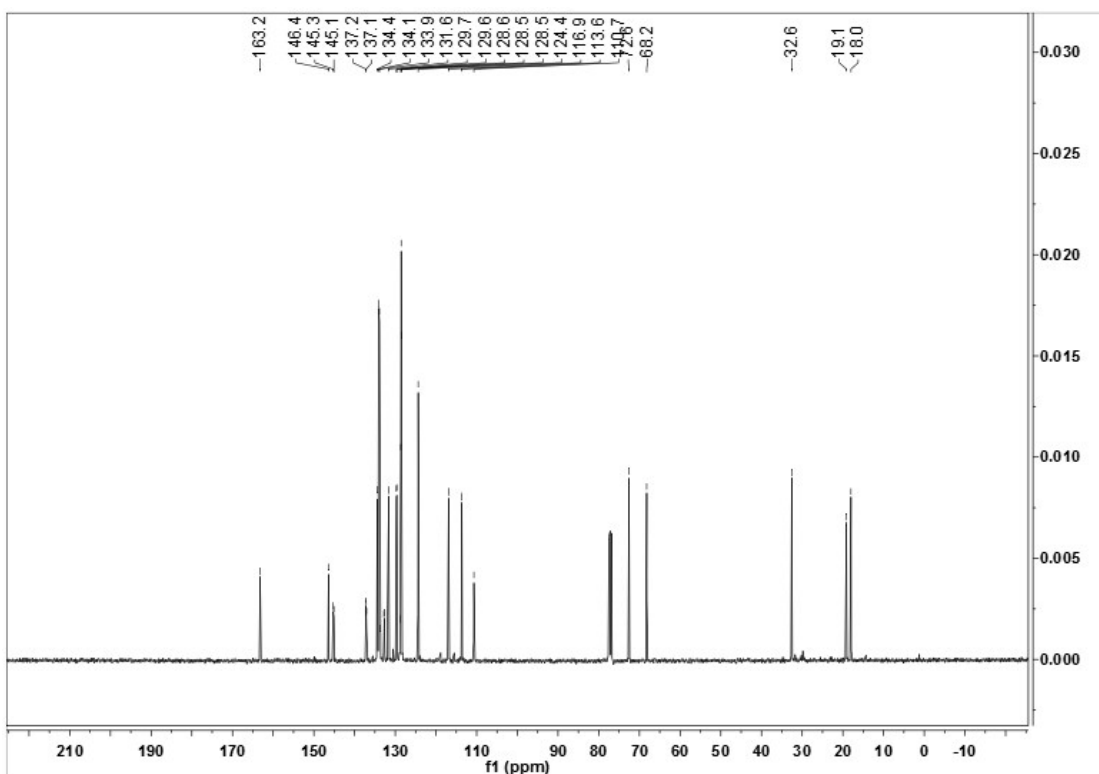


Figure S16 ^{13}C NMR spectrum of **Pd1** (101 MHz, CDCl_3 , 25 °C)

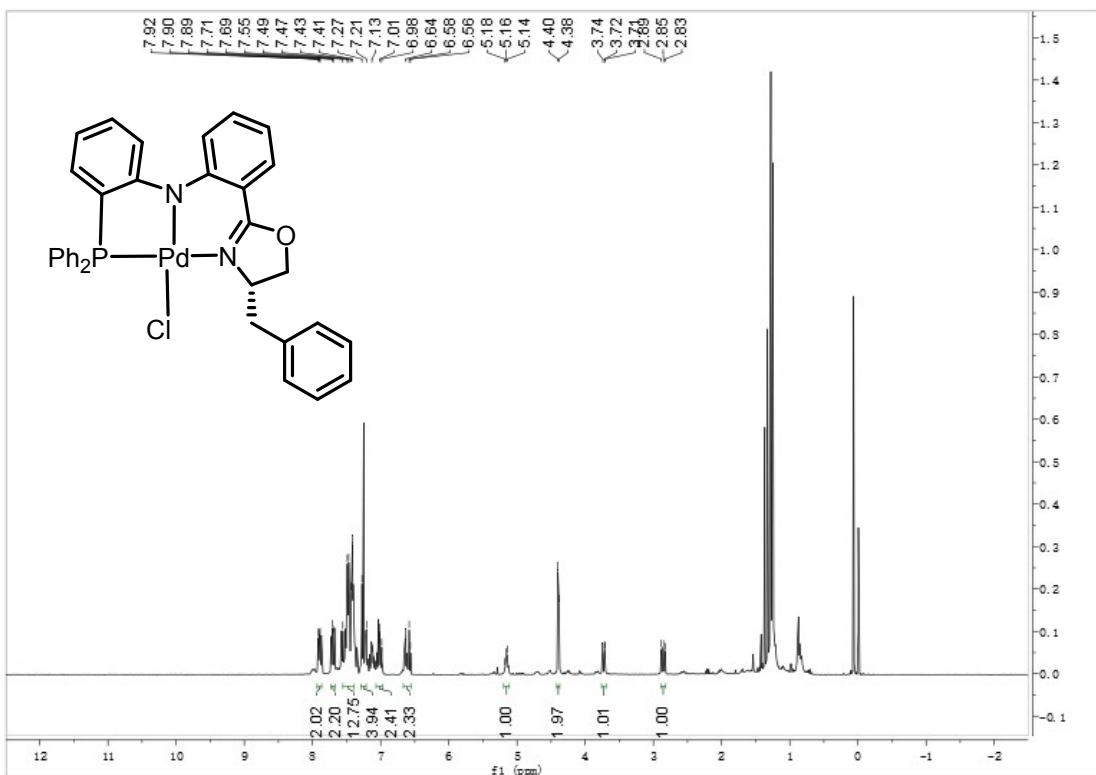


Figure S17 ¹H NMR spectrum of Pd2 (400 MHz, CDCl₃, 25 °C)

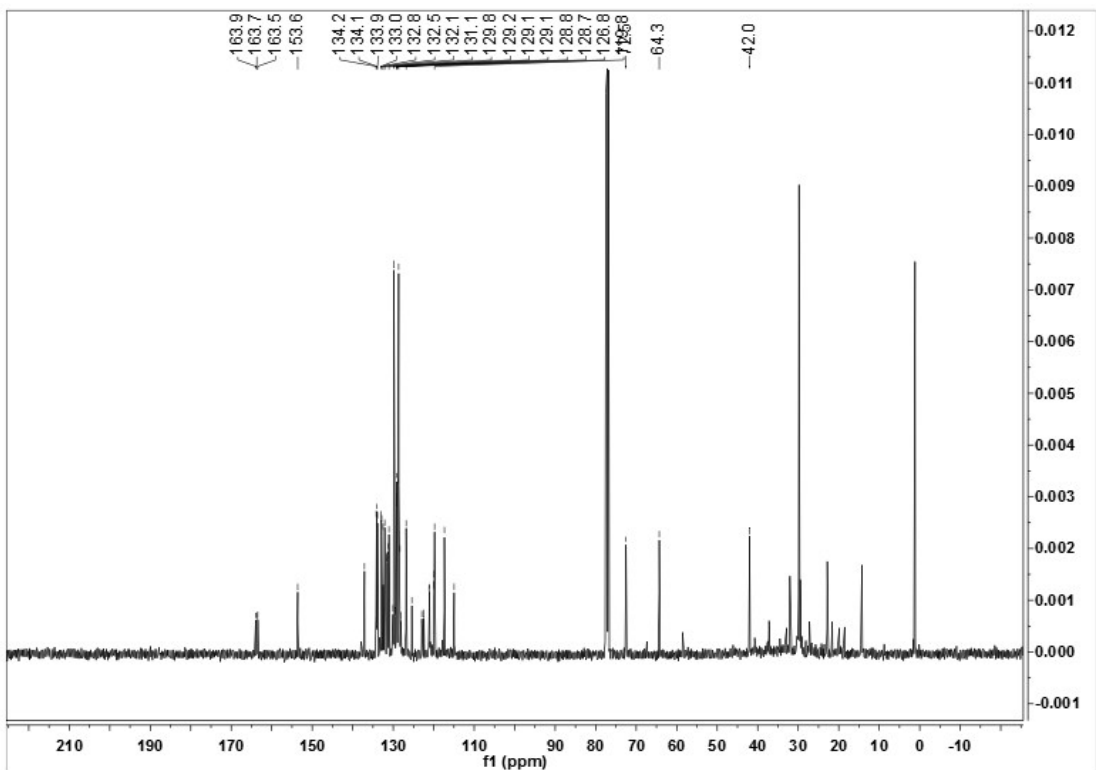


Figure S18 ¹³C NMR spectrum of Pd2 (101 MHz, CDCl₃, 25 °C)

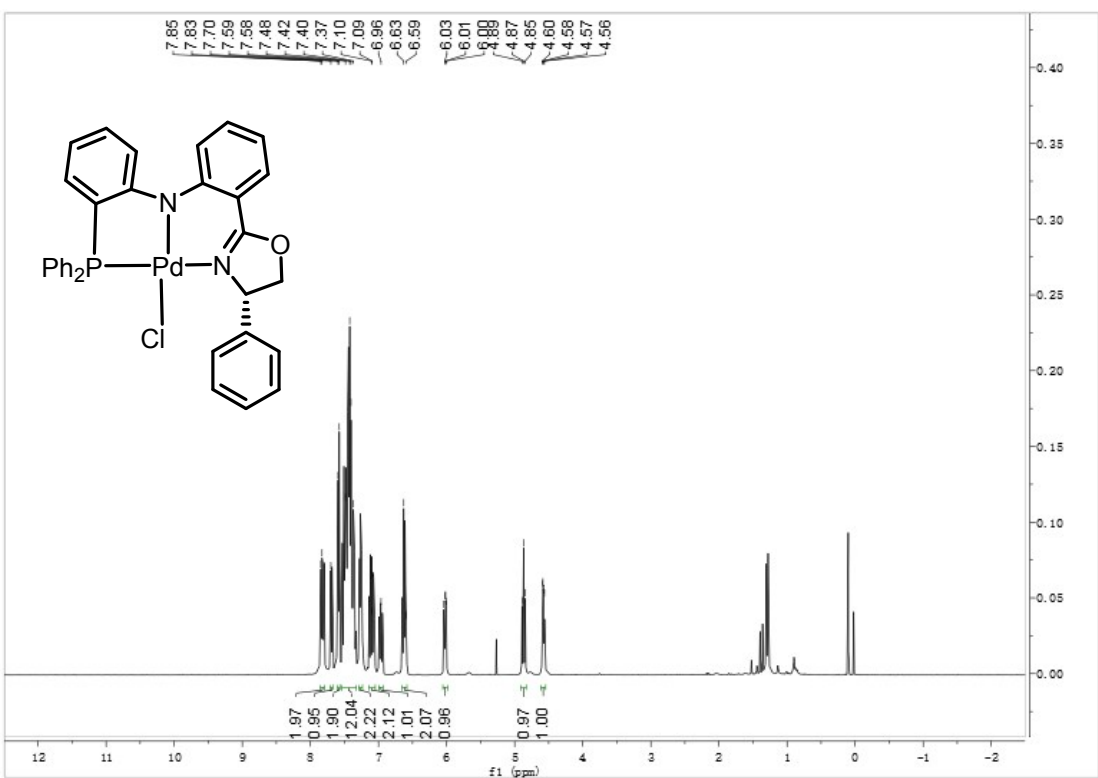


Figure S19 ¹H NMR spectrum of Pd3 (400 MHz, CDCl₃, 25 °C)

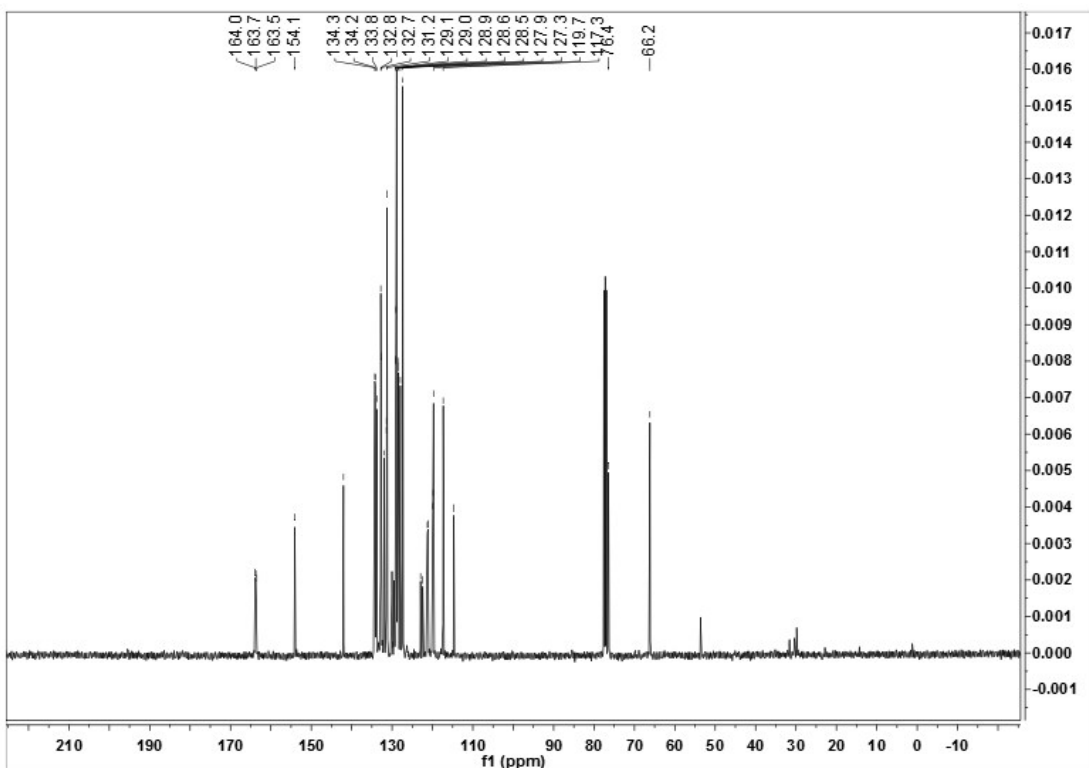


Figure S20 ¹³C NMR spectrum of Pd3 (101 MHz, CDCl₃, 25 °C)

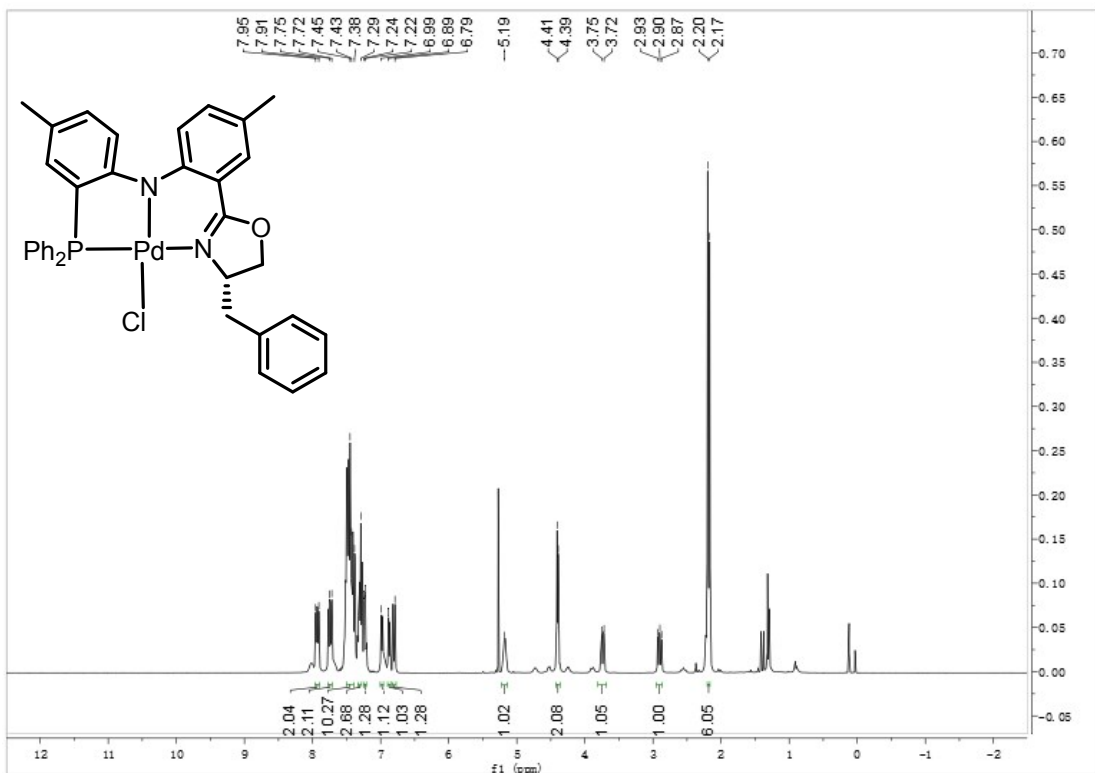


Figure S21 ^1H NMR spectrum of **Pd4** (400 MHz, CDCl_3 , 25 °C)

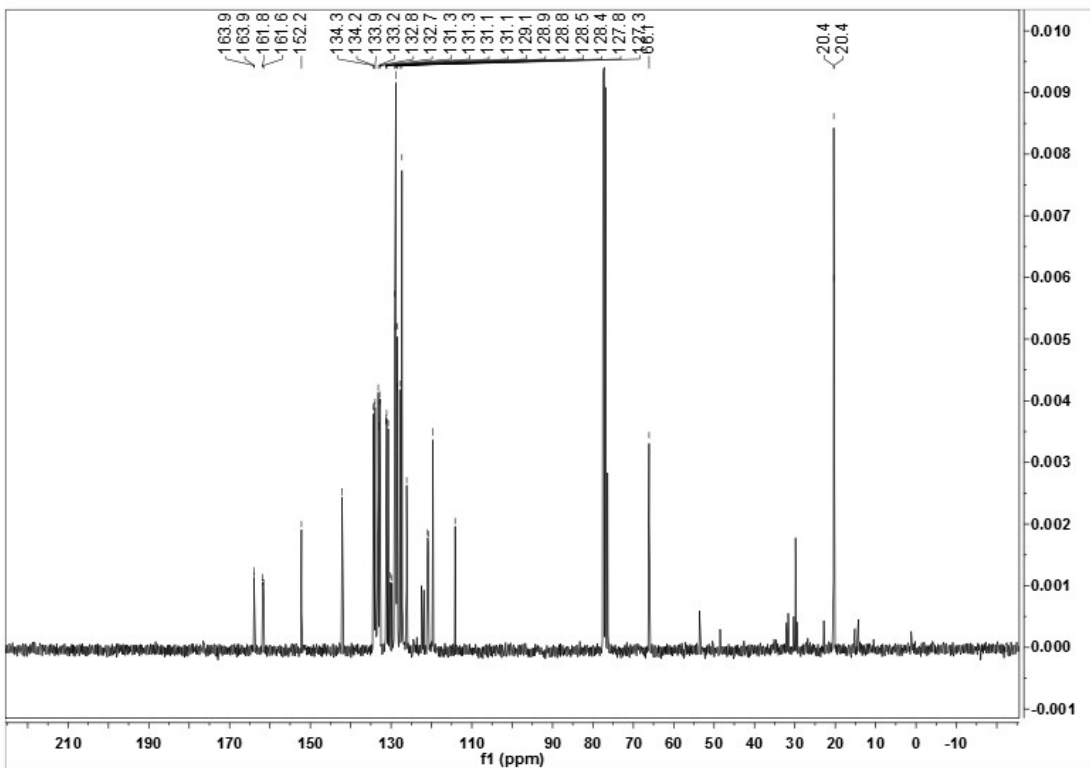


Figure S22 ^{13}C NMR spectrum of **Pd4** (101 MHz, CDCl_3 , 25 °C)

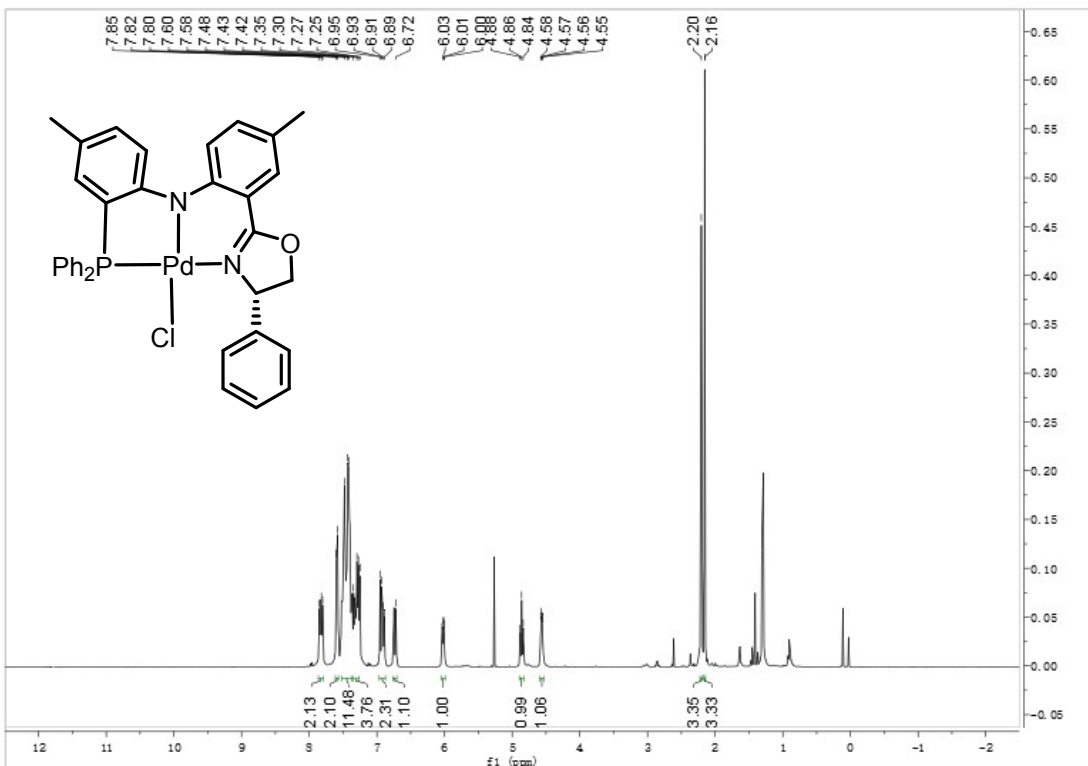


Figure S23 ¹H NMR spectrum of **Pd5** (400 MHz, CDCl₃, 25 °C)



Figure S24 ¹³C NMR spectrum of **Pd5** (101 MHz, CDCl₃, 25 °C)

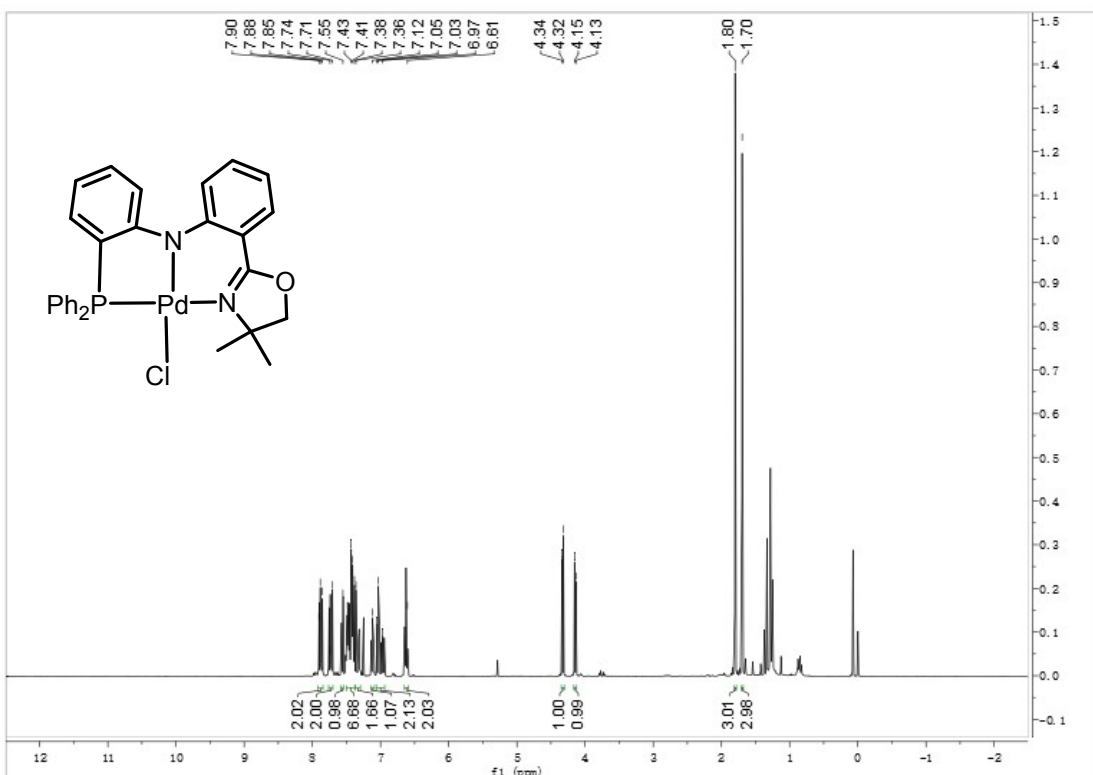


Figure S25 ^1H NMR spectrum of **Pd6** (400 MHz, CDCl_3 , 25 °C)

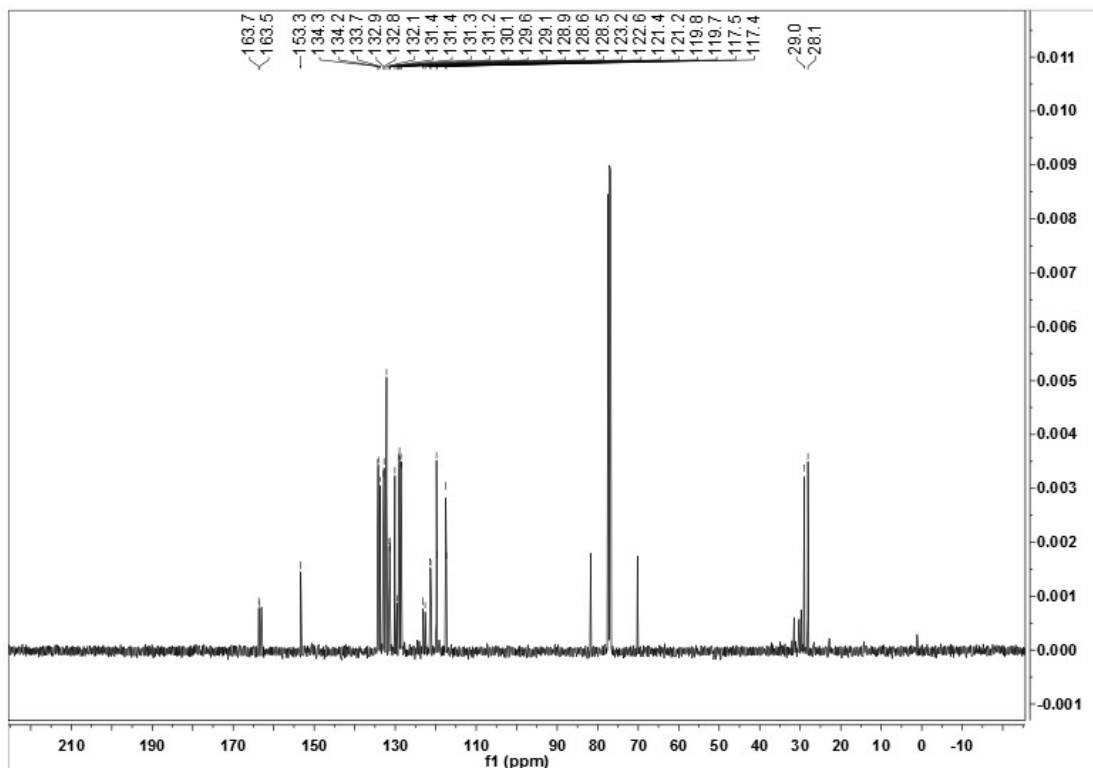


Figure S26 ^{13}C NMR spectrum of **Pd6** (101 MHz, CDCl_3 , 25 °C)

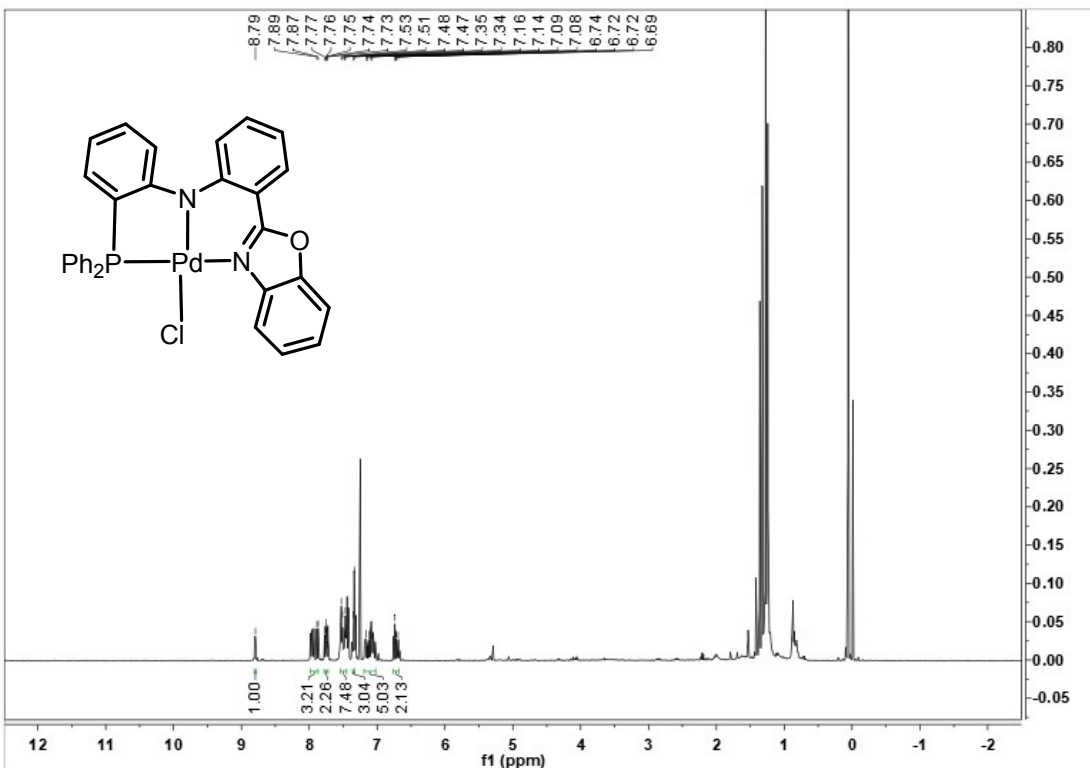


Figure S27 ¹H NMR spectrum of Pd7 (400 MHz, CDCl₃, 25 °C)

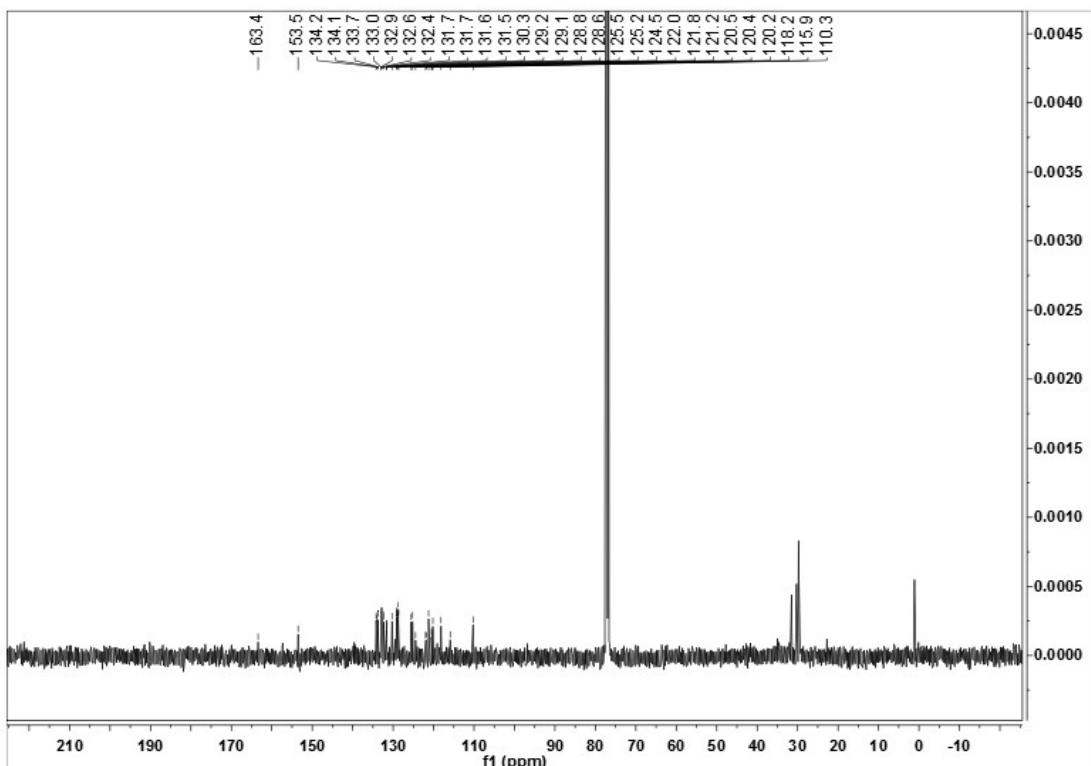


Figure S28 ¹³C NMR spectrum of Pd7 (101 MHz, CDCl₃, 25 °C)

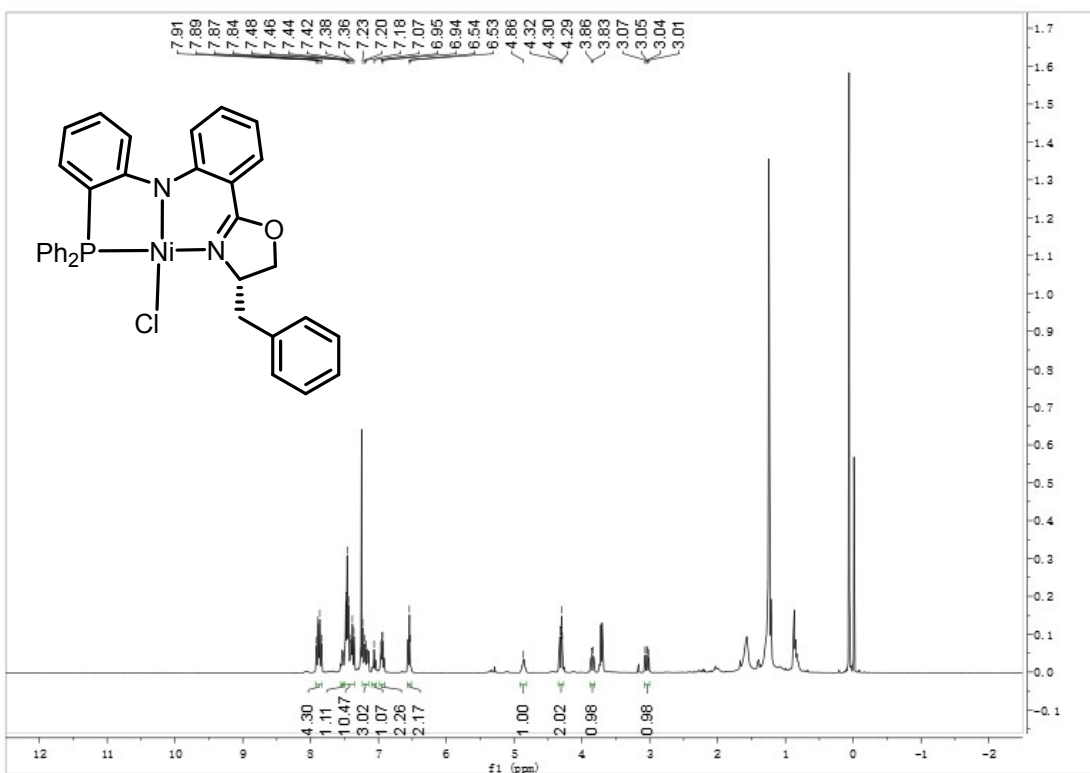


Figure S29 ¹H NMR spectrum of Ni1 (400 MHz, CDCl₃, 25 °C)

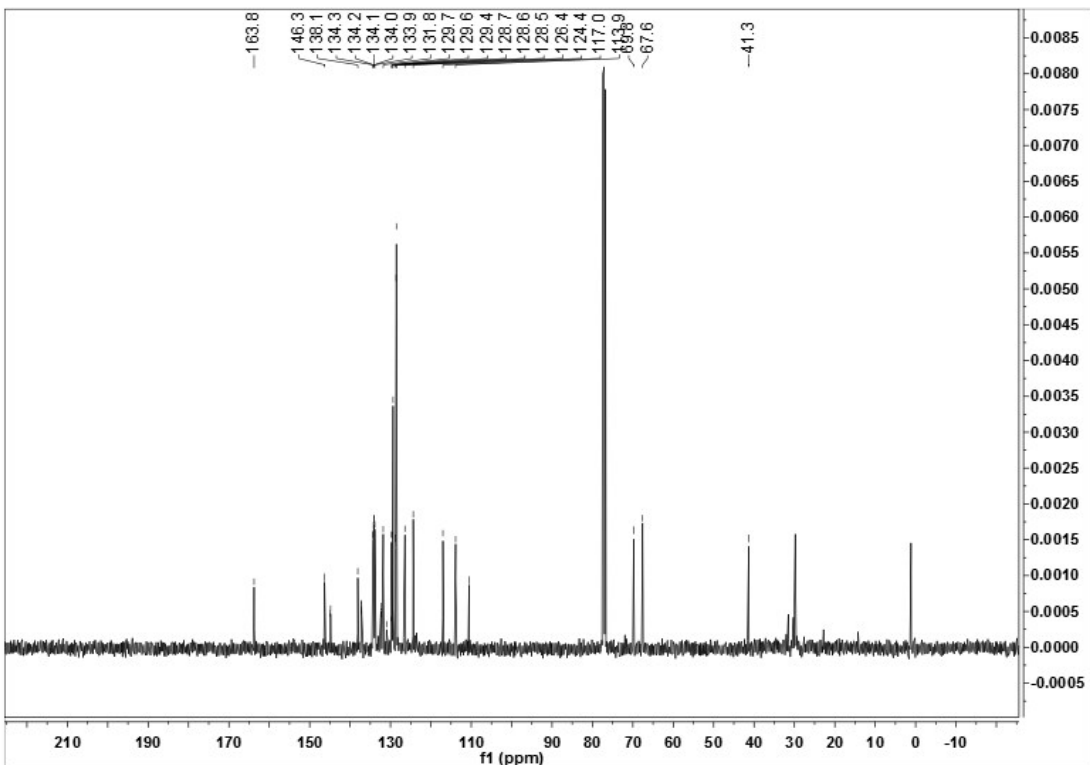


Figure S30 ¹³C NMR spectrum of Ni1 (101 MHz, CDCl₃, 25 °C)

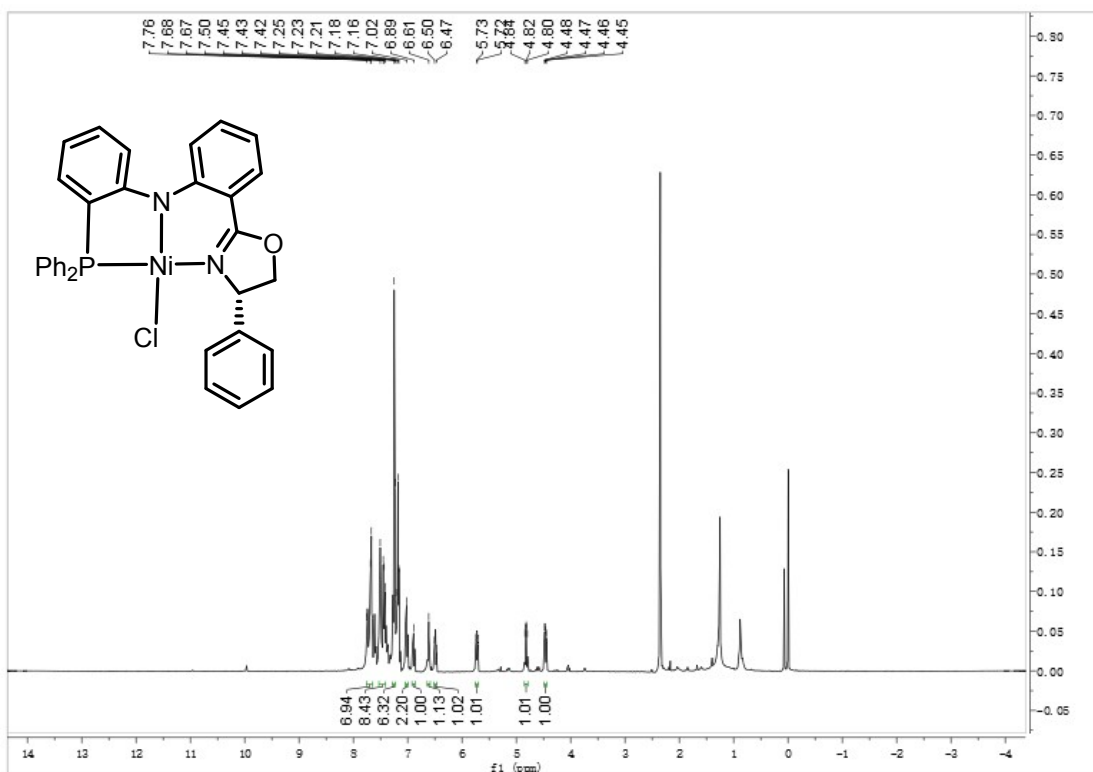


Figure S31 ^1H NMR spectrum of **Ni2** (400 MHz, CDCl_3 , 25 °C)

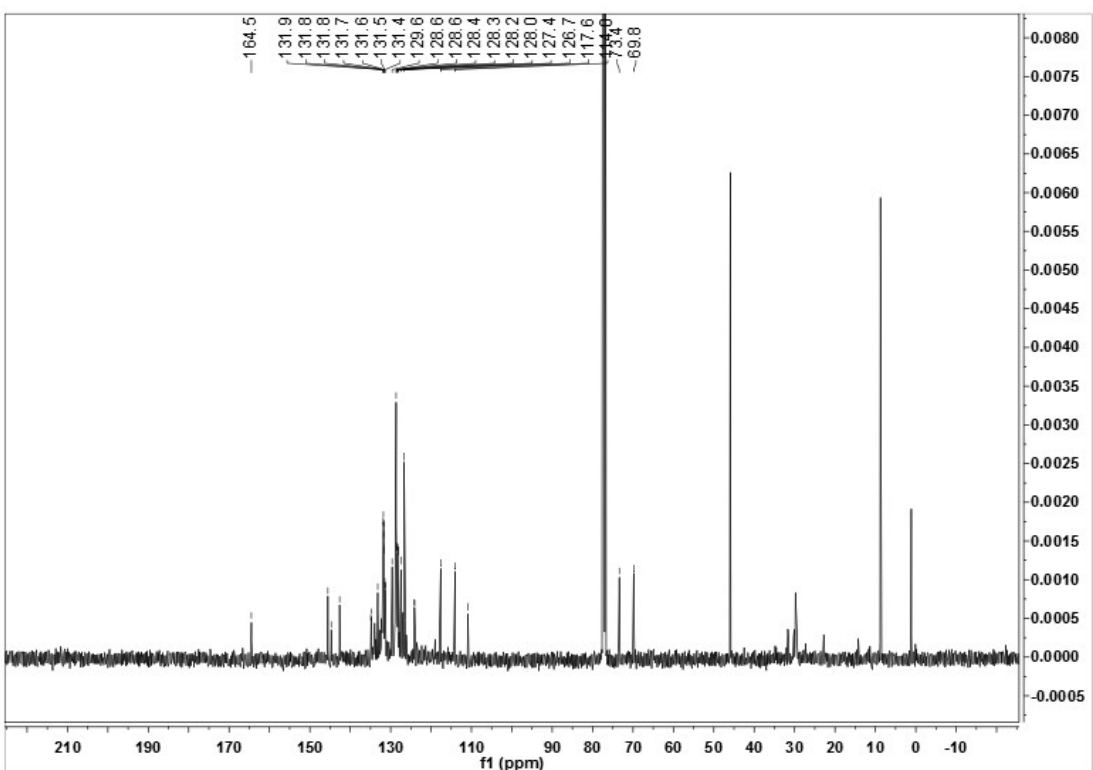


Figure S32 ^{13}C NMR spectrum of **Ni2** (101 MHz, CDCl_3 , 25 °C)

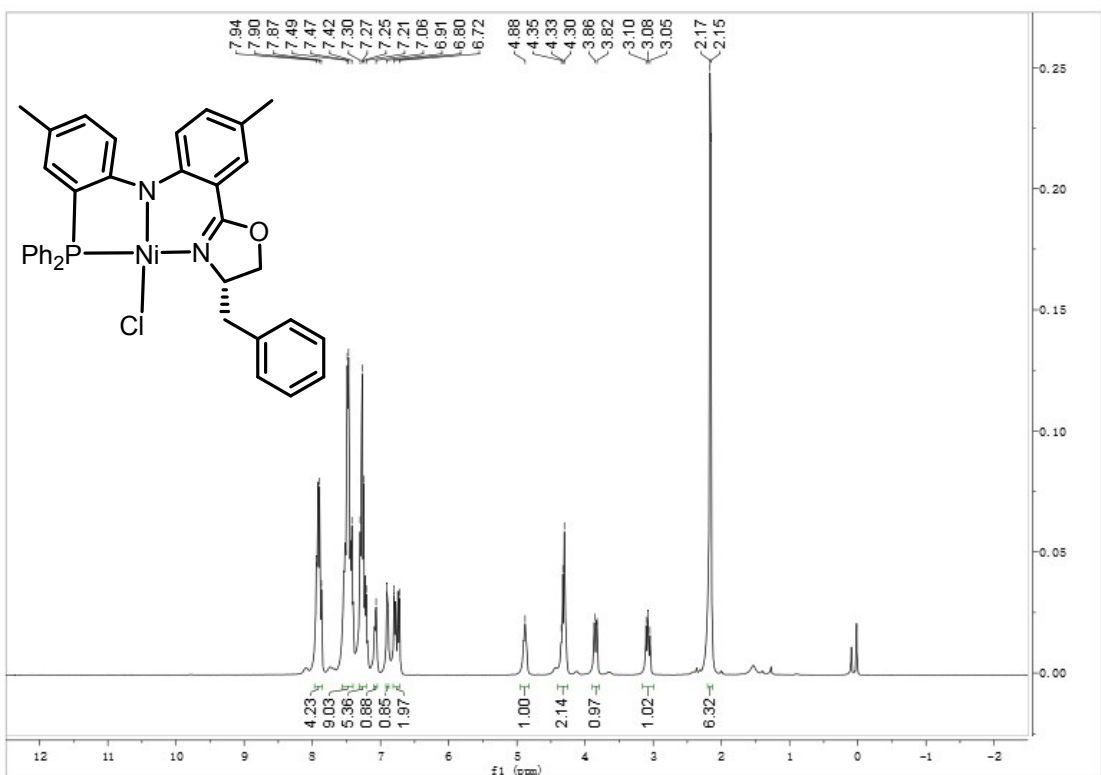
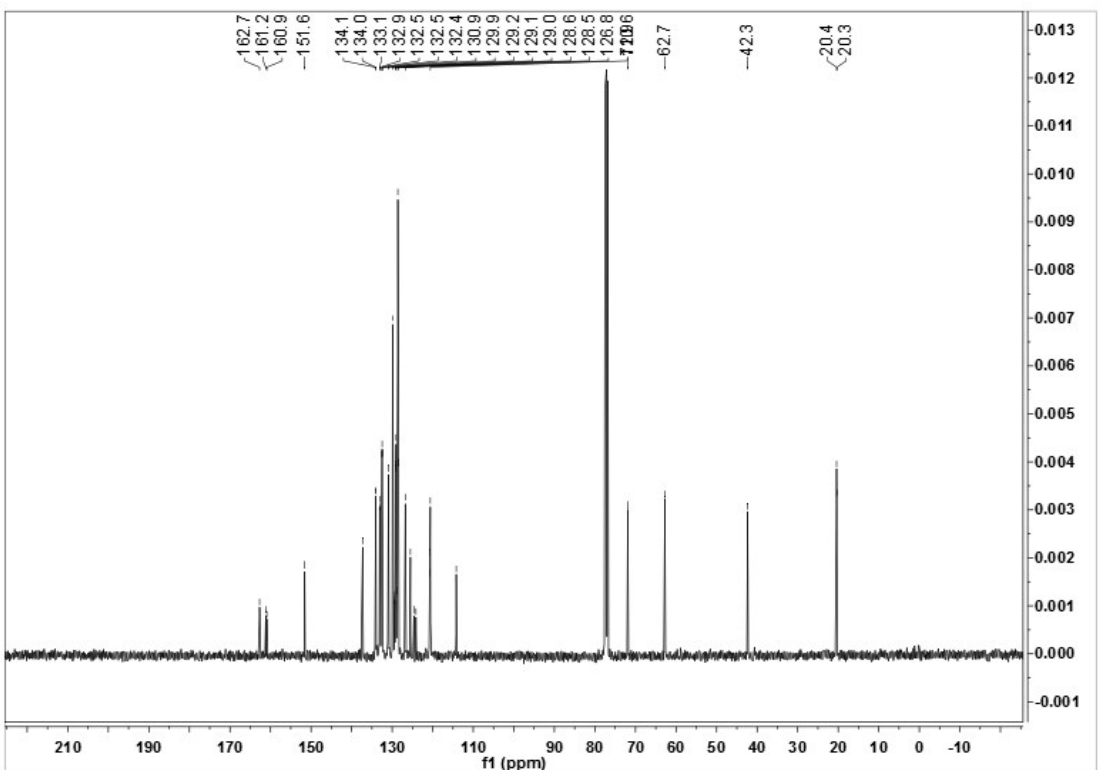


Figure S33 ¹H NMR spectrum of Ni3 (400 MHz, CDCl₃, 25 °C)



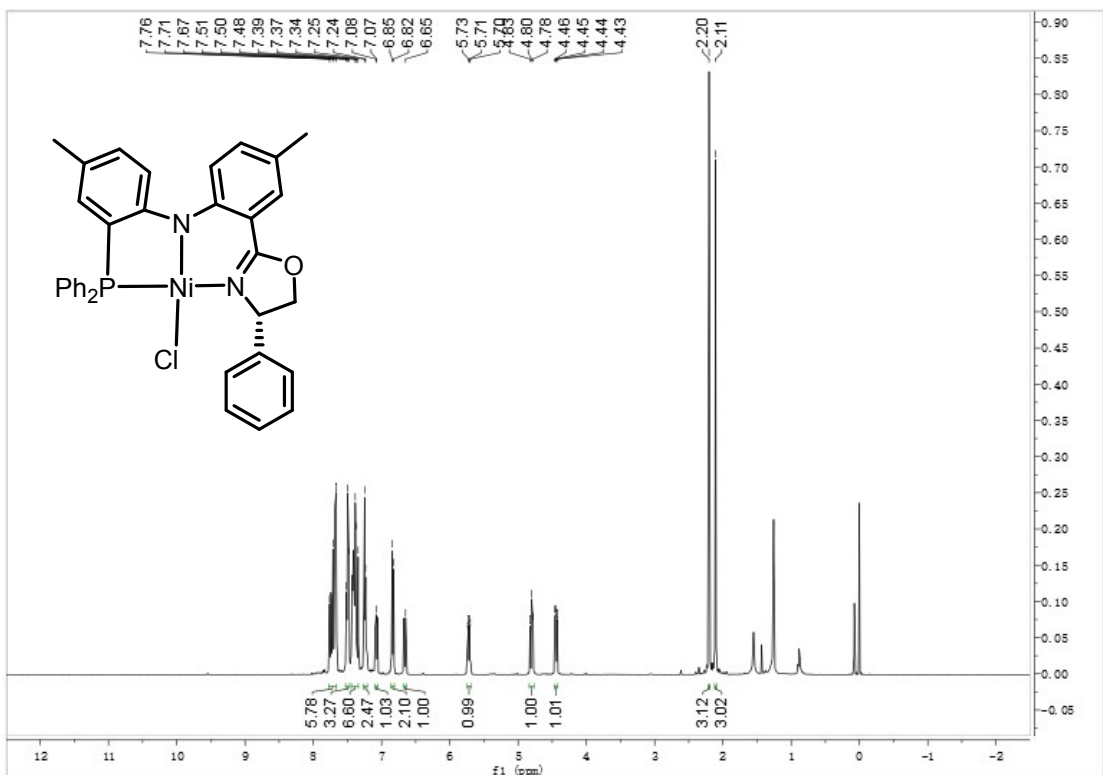


Figure S35 ¹H NMR spectrum of Ni4 (400 MHz, CDCl₃, 25 °C)

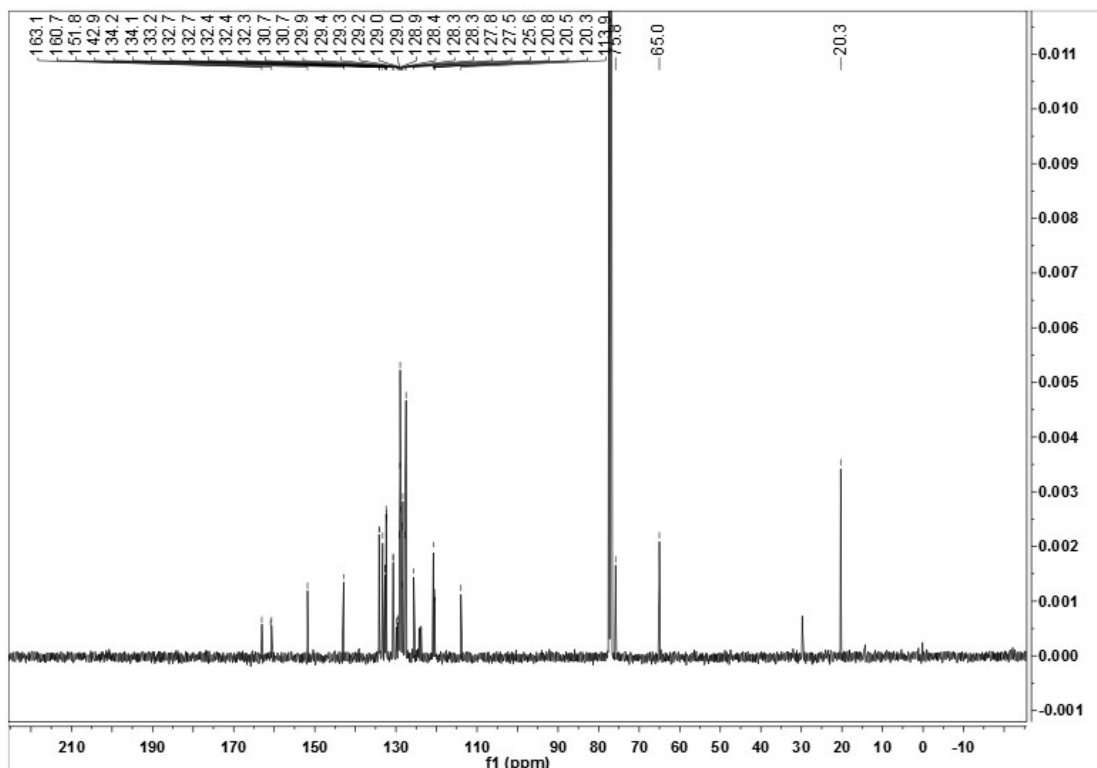


Figure S36 ¹³C NMR spectrum of Ni4 (101 MHz, CDCl₃, 25 °C)

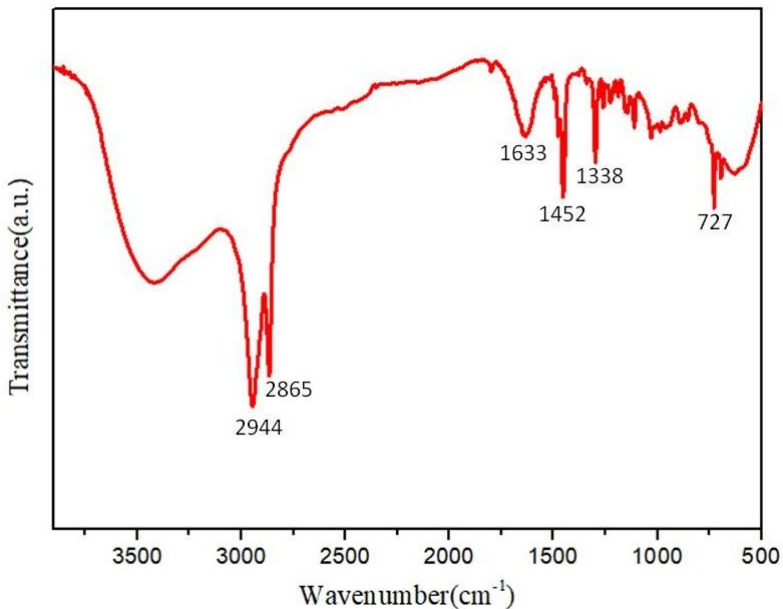
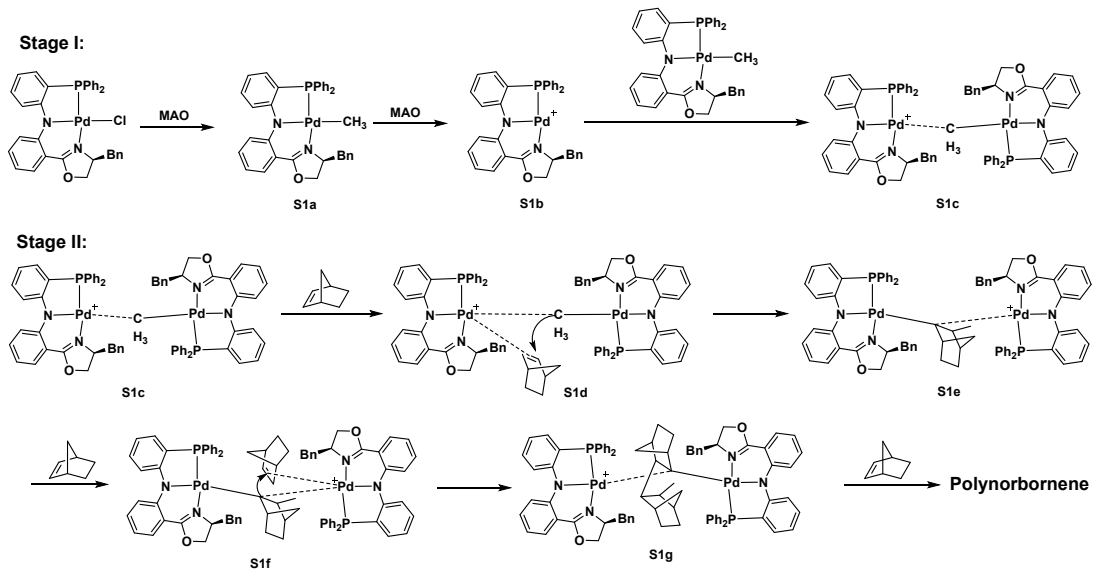


Figure S37 FT-IR spectrum of PNB in Entry 4, Table 1



Scheme S1 Possible mechanism for MAO-activated norbornene polymerization. Excess MAO first alkylates the **Pd2** to form **S1a**, and then further abstracts the methyl group in **S1a** to form cationic **S1b**. The interaction of **S1a** with **S1b** via the -CH₃ bridge forms the active cationic species **S1c** (partly due to the instability of **S1b**), which is the true active centre for polymerization. A norbornene molecule firstly coordinate to the Pd⁺ in **S1c**, and then the methyl group attacks and inserts into the double bond of norbornene to generate **S1e**. After this reaction, the cation center transfers to the another Pd atom and the formed **S1e** acts as a new active centre same

to the role of **S1c** for norbornene polymerization. The following coordination of a new norbornene molecule and insertion of norbornenyl group in **S1e** afford another active centre **S1g**, accompanying with the transformation between the neutral and cationic Pd atoms. Continuous coordination and insertion of norbornene alternatively on the two Pd centres of binuclear compound produce the resultant polynorbornene.

Table S1. Results of Norbornene Copolymerization with Palladium Complexes/Cocatalysts Systems^a

Entry	Monomer	ratio	co-Cat.	[Al]/[Pd]	t / min	Yield / %	Incorp./%	Activity ^b	M _n /x10 ⁴	M _w /M _n
1	VNB	1:1	MAO	7000	300	-	-	-	-	-
2	VNB	1:5	MAO	7000	240	6.55	11.6	10.92	2.28	1.89
3	VNB	1:10	MAO	7000	180	11.71	<1	26.02	2.28	2.43
4	DCPD	1:10	MAO	7000	180	8.54	1.1	18.98	1.20	2.05

^aPolymerization conditions: complex, 1.5 μmol, toluene, V_{total} 10 mL, the ratio of comonomers to norbornene, norbornene 1 g, 25 °C. ^bIn units of 10³ g of PNB (mol of Pd)⁻¹ h⁻¹.

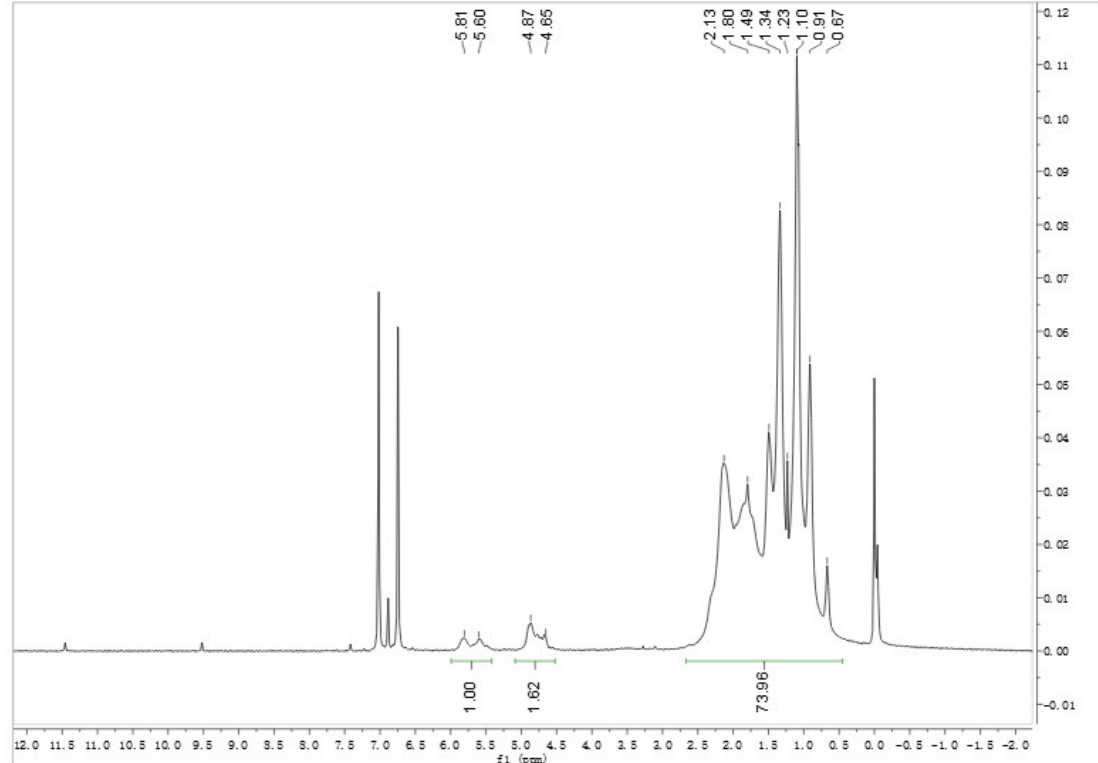


Figure S38 ¹H NMR spectrum of the copolymer of norbornene with VNB (400 MHz, 1,2-Dichlorobenzene- d4, 120°C) in Entry 2, Table S1

Table S2. Summary of the crystallographic data for **Pd1**, **Pd2**, **Pd6** and **Pd7**

	Pd1	Pd2	Pd6	Pd7
Empirical formula	C ₃₀ H ₂₈ ClN ₂ OPPd	C ₃₄ H ₂₉ ClN ₂ OPPd	C ₂₉ H ₂₆ ClN ₂ OPPd	C ₃₁ H ₂₂ ClN ₂ OPPd
Formula weight	605.36	653.41	591.34	611.33
Temperature/K	296(2)	296(2)	296(2)	293(2)
Wavelength/ Å	0.71073	0.71073	0.71073	0.71073
Crystal system	Orthorhombic	Monoclinic	Monoclinic	Triclinic
Space group	P2(1)2(1)2(1)	P2(1)	P2(1)/c	P-1
a/Å	9.347(5)	10.606(11)	14.266(8)	9.616(7)
b/Å	10.065(6)	14.265(14)	11.778(6)	11.057(8)
c/Å	28.656(16)	10.706(11)	17.235(9)	12.628(9)
$\alpha/^\circ$	90	90	90	103.175(8)
$\beta/^\circ$	90	114.708(11)	112.784(6)	99.103(9)
$\gamma/^\circ$	90	90	90	92.477(8)
V/Å ³	2696(3)	1471(3)	2670(2)	1286.5(16)
Z	4	2	4	2
D _c /Mg m ⁻³	1.491	1.477	1.471	1.578
μ/mm^{-1}	0.873	0.806	0.879	0.916
F(000)	1232	666	1200	616
Crystal size/mm ³	0.28 x 0.25 x 0.24	0.21 x 0.20 x 0.07	0.11 x 0.09 x 0.03	0.15 x 0.13 x 0.06
2θ range for data collection/°	2.14 to 25.05	2.09 to 25.05	2.15 to 25.05	2.15 to 25.05
Limiting indices(hkl)	-10, 11; -11, 11; -31, 34	-12, 11; -16, 6; -12, 11	-16, 16; -14, 13; -20, 19	-11, 11; -13, 8; -12, 15
Reflections collected	13926	7431	13451	6541
Independent reflections	4757	4937	4699	4415
R _{int}	0.0186	0.0213	0.0249	0.0168
Completeness to 0/°	25.05 (99.9 %)	25.05 (97%)	25.05 (99.7%)	25.05 (96.9%)
Data/restraints/parameters	4757 / 0 / 327	4937 / 1 / 361	4699 / 0 / 318	4415 / 0 / 335
Goodness-of-fit on F ²	1.080	1.054	1.047	1.187
Final R indexes [I ≥ 2σ (I)]	R1 = 0.0177, wR2 = 0.0434	R1 = 0.0257, wR2 = 0.0590	R1 = 0.0256, wR2 = 0.0590	R1 = 0.0332, wR2 = 0.0894
Final R indexes [all data]	R1 = 0.0182, wR2 = 0.0436	R1 = 0.0285, wR2 = 0.0611	R1 = 0.0333, wR2 = 0.0636	R1 = 0.0407, wR2 = 0.1032
Largest diff. peak/hole / e Å ⁻³	0.192, -0.273	0.363, -0.467	0.296, -0.422	0.713, -0.659

$$R_I = \sum ||F_O| - |F_C|| / \sum |F_O|; wR_2 = [\sum w(F_o^2 - F_c^2)^2 / \sum w(F_o^2)^2]^{1/2}$$